Diffusion-Assisted High-Resolution Direct Femtosecond Laser Writing

Ioanna Sakellari,[†] Elmina Kabouraki,[†,‡] David Gray,[†] Vytautas Purlys,[†] Costas Fotakis,[†,§] Alexander Pikulin,[⊥] Nikita Bityurin,[⊥] Maria Vamvakaki,[†,‡] and Maria Farsari[†,*]

[†]IESL-FORTH, N. Plastira 100, 70013, Heraklion, Crete, Greece, [‡]Department of Materials Science and Technology, University of Crete, Heraklion, Crete, Greece, [§]Department of Physics, University of Crete, Heraklion, Crete, Greece, and [⊥]Institute of Applied Physics, Russian Academy of Sciences, Nizhny Novgorod, Russia

ABSTRACT

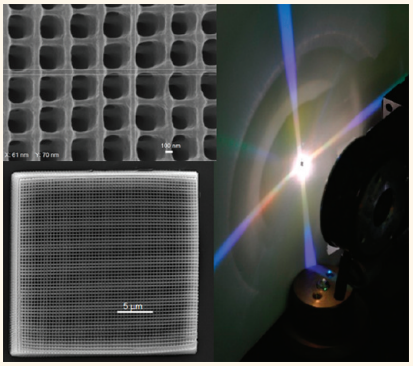

We present a new method for increasing the resolution of direct femtosecond laser writing by multiphoton polymerization, based on quencher diffusion. This method relies on the combination of a mobile quenching molecule with a slow laser scanning speed, allowing the diffusion of the quencher in the scanned area and the depletion of the multiphoton-generated radicals. The material we use is an organic—inorganic hybrid, while the quencher is a photopolymerizable amine-based monomer which is bound on the polymer backbone upon fabrication of the structures. We use this method to fabricate woodpile structures with a 400 nm intralayer period. This is comparable to the results produced by direct laser writing based on stimulated-emission-depletion microscopy, the method considered today as state-of-the-art in 3D structure fabrication. We optically characterize these woodpiles to show that they exhibit well-ordered diffraction patterns and stopgaps down to near-infrared wavelengths. Finally, we model the quencher diffusion, and we show that radical inhibition is responsible for the increased resolution.

KEYWORDS: direct laser writing · multiphoton polymerization · quenching · hybrid materials · photonic nanostructures

Direct laser writing (DLW) by multiphoton polymerization (MPP) has become a powerful tool for the fabrication of fully three-dimensional micro- and nanostructures for microfluidic, biomedical, metamaterial, and photonic applications.[1−5] In DLW, the beam of an ultrafast laser is tightly focused into the volume of a photosensitive material, initiating multiphoton polymerization within the focused beam volume (namely, voxel). By moving the focus of the beam three-dimensionally, arbitrary 3D, high-resolution structures can be written into the volume of the material. By simply immersing the sample in an appropriate solvent, the unscanned, unpolymerized area can be dissolved, revealing the 3D structure.

While DLW is fundamentally the only technique available that can produce readily assembled, fully 3D micro- and nanostructures, its resolution lags behind other competing technologies such as e-beam lithography, where tens of nanometers are routinely achieved. Recently, there has been a lot of research effort to improve this resolution.[6] One method is the use of an inhibiting molecule, such as a quencher, in the photopolymerizable material.[7] In general, photopolymerization is a light-induced reaction that converts a monomer into a solid polymer. This reaction requires the use of an appropriate photoinitiator, a light-sensitive molecule that produces a radical upon irradiation. It is a popular misconception that the highest resolution that can be achieved by a focused light beam is given by Abbe's diffraction limit.[8,9] In fact, this is only valid in reversible, noninvasive procedures, such as imaging. When there is permanent modification of the sample, like in photopolymerization, then there is more than one process involved. To start with, when absorbing the light, the photoinitiator becomes excited and produces radicals; these radicals attack monomer molecules to form macroradicals of the polymer. Finally, the radicals are terminated to give the polymer. Radical termination can be also induced by oxygen and other molecules in the system, known as scavengers. Quenching competes with photopolymerization and is usually considered detrimental to the process. In multiphoton photopolymerization, however, it can be used to circumvent the diffraction limit and produce

* Address correspondence to mfarsari@iesl.forth.gr.

Received for review November 16, 2011 and accepted February 10, 2012.

Published online February 10, 2012
10.1021/nn204454c

structures of very high resolution. This can be done by modifying the light intensity at the focal point so that the light-produced radicals, whose spatial concentration is proportional to the square of the light intensity, exceed the quenchers and initiate polymerization only at the area where the exposure energy is larger than the threshold. In this case, the diffraction limit becomes just a measure of the focal spot size, and it does not really determine the polymerization voxel size (Figure 1a).

While, however, oxygen or additional quenchers reduce the absolute number of radicals, it should be possible to achieve a similar effect by simply reducing the laser power. Indeed, efforts to date to improve resolution using quenchers have marginally increased the resolution of single, suspended lines.[7,10] However, they have not produced any high-resolution 3D structures. More importantly, they have not reduced the distance between high-resolution lines. As described in detail by Fischer and Wegener,[11] the biggest challenge in DLW not yet addressed is not in the creation of subdiffraction features, but subdiffraction gaps between features. When attempting to form two features at subdiffraction distance, the polymerization threshold is also exceeded in the interstice between the features due to the diffraction-limited widths of the absorbed energy distributions (Figure 1b). This is a geometrical effect that cannot be easily overcome by any physical or chemical mechanism providing the polymerization threshold. A nondiffusing quencher simply increases the polymerization threshold, as the absorbed photons are partly wasted to neutralize the quencher. Diffusion of the free radical can make the spatial resolution even worse by causing indirect polymerization even in unexposed areas.[12]

One method that has successfully and substantially increased the resolution not only of single lines but also of structures is DLW inspired by stimulated-emission-depletion (STED) fluorescence microscopy.[13,14] In STED-DLW, two laser beams are used; one is used to generate the radicals, and the second beam to deactivate them. Several schemes have been proposed including single-photon (rather than multiphoton) excitation,[15] a one-color scheme,[16] and a multiphoton two-color scheme.[11,17] In addition to increasing the resolution, the possibility to shape the deactivating beam allows the very precise control of the voxel shape and, therefore, the polymerization shape. Woodpiles with 350 nm intralayer periodicity and clear stopgaps have been fabricated using this method, while structures with 250 nm intralayer periodicity show evidence of stopgaps.[11] However, the implementation of DLW-STED is complicated, requiring very fine beam control and specialized photoinitiators that have not only high two-photon cross-section but also high fluorescence quantum efficiency.[11,18]

In this paper, we show that it is possible to increase the resolution of multiphoton polymerization

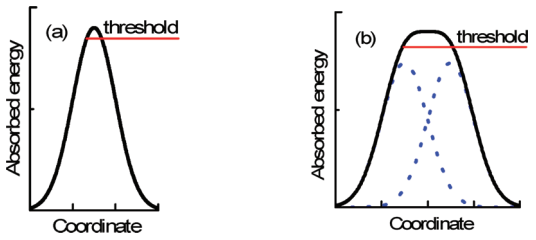

Figure 1. (a) Formation of a single subdiffraction-sized feature is possible due to the polymerization threshold. (b) Formation of two features at subdiffraction distance is limited by tails of the distributions of the energy absorbed during scans (blue, dotted lines). The total absorbed energy (black line) exceeds the threshold not only where the nanofeatures are expected to form but also in the interstice.

by employing a scheme based on quencher diffusion, in a chemical equivalent of STED. This is based on the combination of a mobile quenching molecule and a slow laser scanning speed, allowing the diffusion of the quencher in the scanned area, the depletion of the generated radicals, and the regeneration of the consumed quencher. The material we use is an organic–inorganic hybrid material, which has been shown to structure accurately and with minimal distortion.[3,19–21] The scavenger, 2-(dimethylamino)ethyl methacrylate, is an amine-based photopolymerizable monomer which becomes part of the polymer backbone upon the fabrication of the structures. The addition of this quencher increases the resolution without compromising the mechanical stability of the structures, offering in addition the possibility to selectively metalize these structures.[22,23] We structure the hybrid material with and without the quencher to fabricate 3D photonic crystal woodpile structures using similar conditions, and we show that when using the quencher, it is possible to fabricate woodpile structures with 400 nm intralayer period. This is the lowest woodpile period achieved to date, using a single laser beam.[11] Using a similar material without the quencher the lowest intralayer period reported is 900 nm for woodpile and 700 nm for spiral photonic crystals.[21] We optically characterize these woodpile structures and we show that they exhibit well-ordered diffraction patterns and stopgaps down to near-infrared wavelengths. Finally, we model the quencher diffusion, and we show that radical inhibition is responsible for the increased resolution.

RESULTS AND DISCUSSION

The photonic structures described here are woodpile photonic crystals. As already described by several groups,[24–26] diffraction channels for normal incidence are open when the incident wave vector **k** is larger in magnitude than any of the 2D reciprocal lattice vectors, **g**, of the planes parallel to the crystal surface. A diffraction cutoff is observed whenever $|\mathbf{g}| = |\mathbf{k}|$. For a square lattice, writing **g** as a linear combination of a set

of 2D primitive reciprocal lattice vectors ($\mathbf{b}_1$,$\mathbf{b}_2$), *i.e.* $\mathbf{g} = p\mathbf{b}_1 + q\mathbf{b}_2$, p, q integers, the cutoff condition is met for

$$\frac{d}{\lambda} = \frac{1}{n}\sqrt{p^2+q^2}$$

where n is the refractive index of the diffraction medium, λ is the wavelength of the incident radiation, and d is the periodicity in the planes perpendicular to the propagation direction. In air ($n = 1$) four diffraction channels open, corresponding to

$$(p, q) = (1, 0), (0, 1), (-1, 0), (0, -1)$$

when .

$$\frac{d}{\lambda} \geq 1 \Rightarrow d \geq \lambda$$

In the same manner, a second set of diffraction spots appears for

$$(p, q) = (1, 1), (1, -1), (-1, 1), (-1, -1)$$

when $d > \sqrt{2}\lambda$.

As it can be seen in Figure 2c, in the case of d = 1700 nm, the whole visible spectrum is diffracted as both conditions $d > \lambda$ and $d > \sqrt{2}\lambda$ hold; thus both sets of diffraction channels are observed. The first set of four diffraction spots form the characteristic cross around the forward transmitted beam, whereas the second set of diffraction spots appears along the diagonal directions. The diffraction cutoff starts to become more pronounced as one moves to unit cells close to the visible spectral range, such as for d = 600 nm and d = 500 nm (Figures 3 and 4, respectively), where one can clearly observe the cutoff of the "red part" of the visible. The same situation holds as one moves from d = 500 nm to d = 400 nm (Figure 5), where a cutoff exists for the "red" and the "green part" of the visible spectrum. As the second condition is not met for any visible wavelength for woodpiles with d < 600 nm, no diagonal spots are observed in the diffraction patterns shown in Figures 3c, 4c, and 5c.

Furthermore, for the case of our woodpile structure with d = 400 nm, the characteristic cross is not clearly seen. Instead of the four diffraction channels along two orthogonal directions, only two are observed along a single direction. However, the sharpness of the diffraction spots indicates the long-range order inherent to periodic photonic crystals due to their translational symmetry. This is in accordance to the scanning electron microscopy (SEM) image taken, where structural deformation due to shrinkage is evident. This is further supported by the optical response measured (Figure 5d). Theoretical calculations made using the MPB software package[27] for rod width $w = 0.176c$, refractive index n = 1.52, and rod height $h = 0.5c$ are shown schematically in Figure 5e. The band gap is located for a normalized frequency of $c/\lambda \approx 0.8$, that is, for a vacumn wavelength

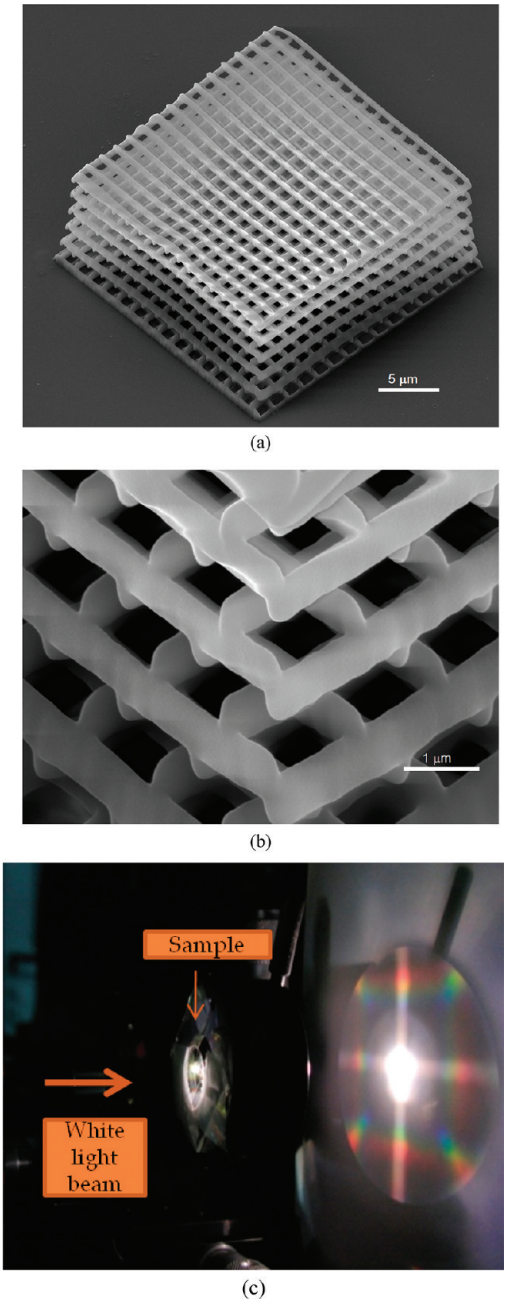

Figure 2. (a) 3D woodpile structure with 1700 nm interlayer periodicity. (b) Detail of the structure. (c) Diffraction pattern generated when a white-light beam goes through the woodpile structure.

of ~710 nm, which is about 100 nm blue-shifted in relation to the transmittance dip measured experimentally (~820 nm). In addition, the diffraction cutoff is located at $c/\lambda \approx 1.414 \geq d$ = 400 nm; thus the other two set of spots may correspond to a higher order partial band gap located at $c/\lambda \approx 0.966$ and higher.

It is worth noting in this case that the highest resolution achieved is of the order of 100 nm (Figure 5b), lower than in the case of the 500 nm interlayer periodicity, where the line width measured was approximately 70 nm Figure 4b. While the difference is small and not enough to draw any conclusions, this

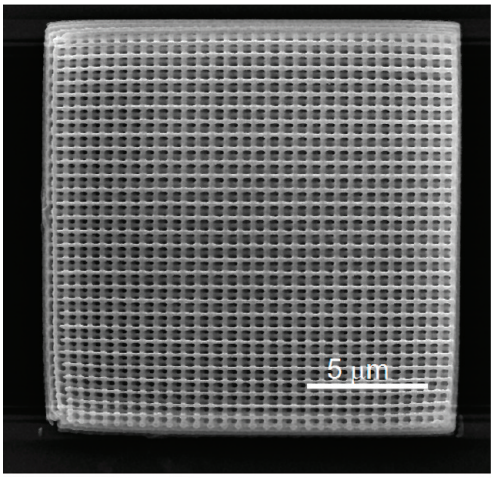

(a)

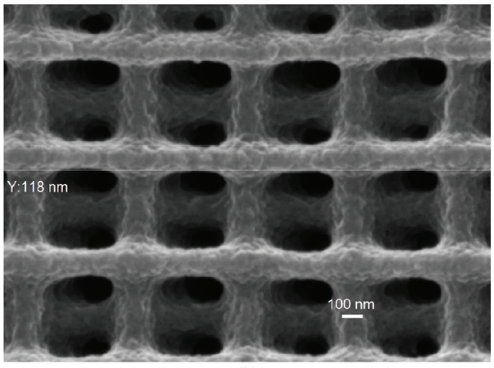

(b)

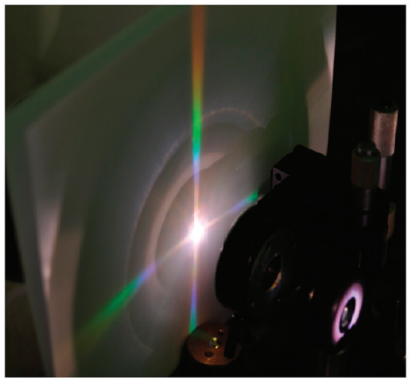

(c)

Figure 3. 3D woodpile structure with 600 nm interlayer periodicity: (a) the whole structure; (b) structure detail; (c) diffraction pattern generated when a white-light beam goes through the woodpile structure.

(a)

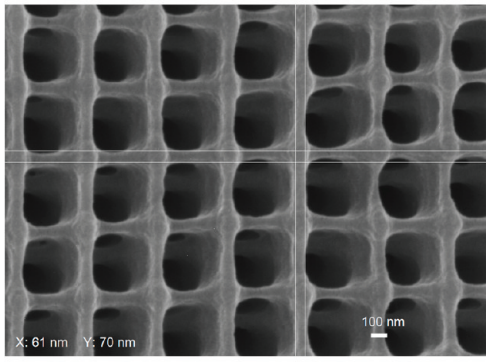

(b)

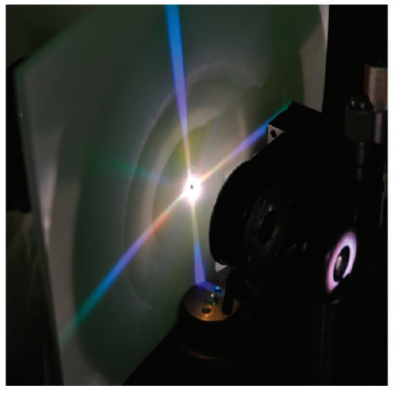

(c)

Figure 4. 3D woodpile structure with 500 nm interlayer periodicity: (a) the whole structure; (b) structure detail; (c) diffraction pattern generated when a white-light beam goes through the woodpile structure.

reduced resolution is possibly due to underexposed areas photopolymerizing due to radical diffusion.

Figure 6 shows a woodpile structure with 500 nm interlayer periodicity, fabricated using the same material without the quencher, *i.e.*, the material described in ref 19. The fabrication conditions were kept the same as previously. In this case however, the intralayer gaps are fully polymerized, and the woodpile in fact is a solid polymer block, allowing us to conclude that the increased resolution is due to the quencher addition.

The use of a quencher not only allows the writing of woodpile structures with lower intralayer periodicity but also allows the writing of finer structures. The resolution of the material without the quencher was studied in detail in ref 20; there, the smallest lateral resolution achieved, even when shrinkage was employed, was 150 nm. Using the quencher, 80–100 nm features are routinely achieved, and 60 nm features have also been fabricated (Figure 4b). Thinner features should also been possible. Fluctuations that rely on percolation-like transition are considered in ref 28. It is not known, however, what

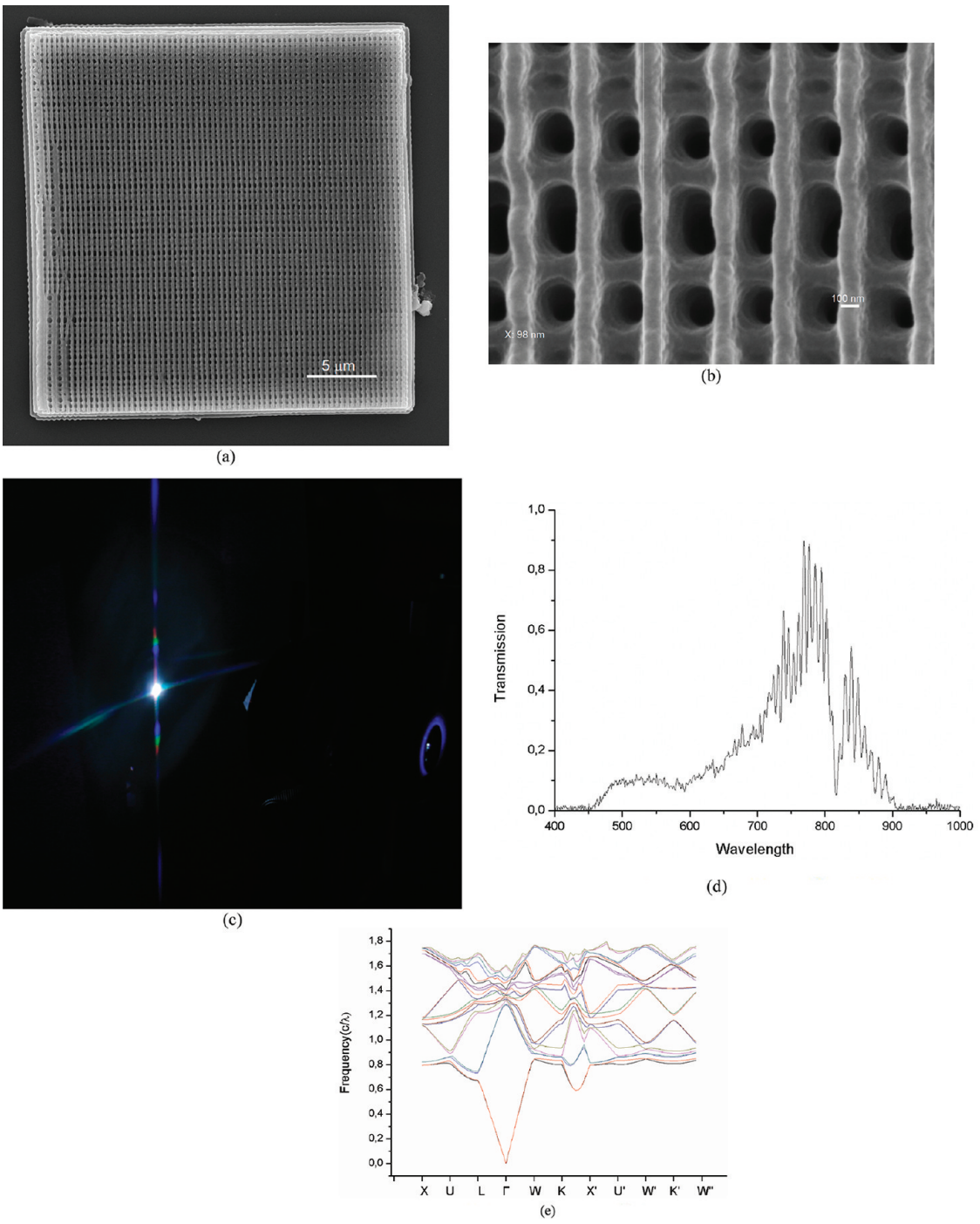

Figure 5. 3D woodpile structure with 400 nm interlayer periodicity: (a) the whole structure, (b) structure detail, (c) diffraction pattern generated when a white-light beam goes through the woodpile structure; (d) measured band gap; and (e) the band calculations.

the effects of thermal or local concentration fluctuations are.

DISCUSSION

Diffusion is a nonlocal factor that, in application to DLW, can cause the energy of light absorbed in one domain of the medium to have a final effect in another domain. Hence, pronounced diffusion weakens the concept of a polymerization threshold, and thus diffusion can potentially help to overcome the limitation on making features at subdiffraction distances. Whereas the diffusion of small radicals as well as macromolecules can be detrimental to spatial resolution, the diffusion of the quencher, which inhibits the polymerization, can have a positive effect.

One of the prominent positive effects of diffusion is the recovery of the initial quencher spatial concentration after irradiation. When writing two adjacent lines, the quencher in the interstice is consumed. When the lines are written at subdiffraction distance to each other,

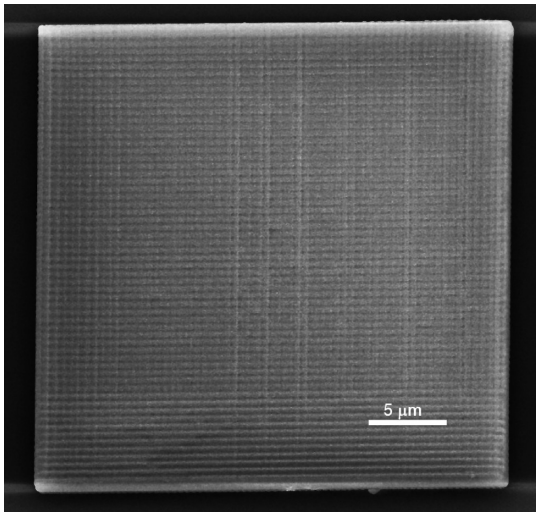

Figure 6. 500 nm intralayer periodicity woodpile structure fabricated using the employed hybrid material without adding a quencher. In this case the interlayer gaps have fully polymerized, resulting in the structure being a solid block.

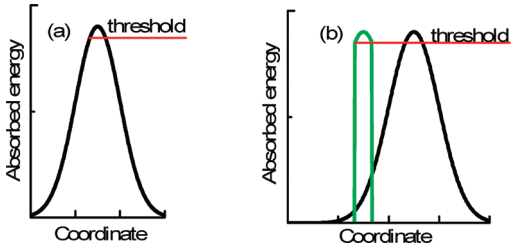

Figure 7. (a) Formation of a single feature. (b) Formation of the second feature at subdiffraction distance from the first one assisted by quencher diffusion. The energy absorbed during the first scan causes both the consumption of the quencher and the formation of the polymer feature. Since the quencher is diffusion-regenerated between scans, the only effect of the irradiation that remains is the formation of the polymer feature (green line). This allows creation of the second feature at the subdiffraction distance.

the quencher in the interstice is totally consumed and the polymerization is started as though it was a single feature, as seen in Figure 1b. However, when the quencher is recovered to its initial concentration before writing of the next neighboring line, such limitation of the spatial resolution is relaxed (Figure 7).

In our experiments, the addition of a quencher causes major improvement in the spatial resolution of written lattices. This means that the quencher not only changes the level of the polymerization threshold but also affects the polymerization nonlocally due to diffusion. The quencher used, DMAEMA, is not attached to the inorganic network, so it can diffuse. The time needed to write a single line of length l_{line} = 30 μm within the photonic crystal with scanning velocity v = 20 μm/s is t_{line} = 1.5 s. As the diffusion coefficient of DMAEMA is $D_Q = 10^{-5}$–10^{-8} cm^2/s, its estimated time of diffusion at the distance of d_{period} = 400 nm between the lines becomes $t_{diff1} = d^2_{period}/D_Q$ that is between 1.6×10^{-4} s and 1.6×10^{-1} s. That is, $t_{diff1} \ll t_{line}$, and therefore the quencher initial concentration recovers between line scans.

With N.A. = 1.4 and λ = 800 nm the beam radius is $r_{beam} \approx 180$ nm. Therefore, the irradiation time of a particular point is $t_{irr} = 2r_{beam}/v = 8 \times 10^{-2}$ s. The estimated time of diffusion of DMAEMA through the irradiated domain is $t_{diff2} = r^2_{beam}/D_Q$ that is between 3.2×10^{-5} s and 3.2×10^{-2} s. That is, $t_{diff2} < t_{irr}$, and thus diffusion is important during single line scans as well.

To understand the effect of the quencher diffusion during the line scans, let us now consider a basic photopolymerization model. The evolution of the spatial distributions of the number densities of the quencher molecules (Q), free radicals (R), and free monomer molecules (M) can be modeled by the following equation set:

$$\frac{\partial R}{\partial t} = S(\bar{r}, t) - k_{tQ}QR \quad (1)$$

$$\frac{\partial Q}{\partial t} = D_Q \Delta Q - k_{tQ}QR \quad (2)$$

$$-\frac{\partial M}{\partial t} = k_p RM \quad (3)$$

Free radicals are generated as a result of the absorption of laser light by the photoinitiator. For two-photon absorption, the source term is proportional to the square of the local field intensity, I, pulse duration t_p, and pulse repetition rate R_p: $S \propto I^2(\vec{r},t)t_pR_p$. As a result of the quenching reaction, both the quencher and the radical are consumed with the reaction rate k_{tQ}. The diffusion coefficient of the quencher is D_Q, Δ, is the Laplacian. The polymerization rate is given by eq 3, being proportional to the monomer number density, M, the radical number density, and the propagation constant k_p. The conversion

$$p = \frac{M_0 - M}{M_0}$$

indicates the degree of polymerization (here, M_0 is the starting number density of the monomer).

Since the line scan is much slower than the diffusion of the quencher, *i.e.*, $t_{diff2} \ll t_{irr}$, one can consider long-lasting irradiation with a constant in time point-like source. For simplicity, we take the spherically symmetric Gaussian source:

$$S = S_0 \exp(-r^2/2L^2) \quad (4)$$

Due to diffusion, the consumption of the quencher in the irradiated volume can be compensated by its transfer from nonirradiated domains. In such a balanced state the quencher number density distribution is maintained constant in time: $\partial Q/\partial t \equiv 0$. Examples of such calculated distributions are shown in Figure 8.

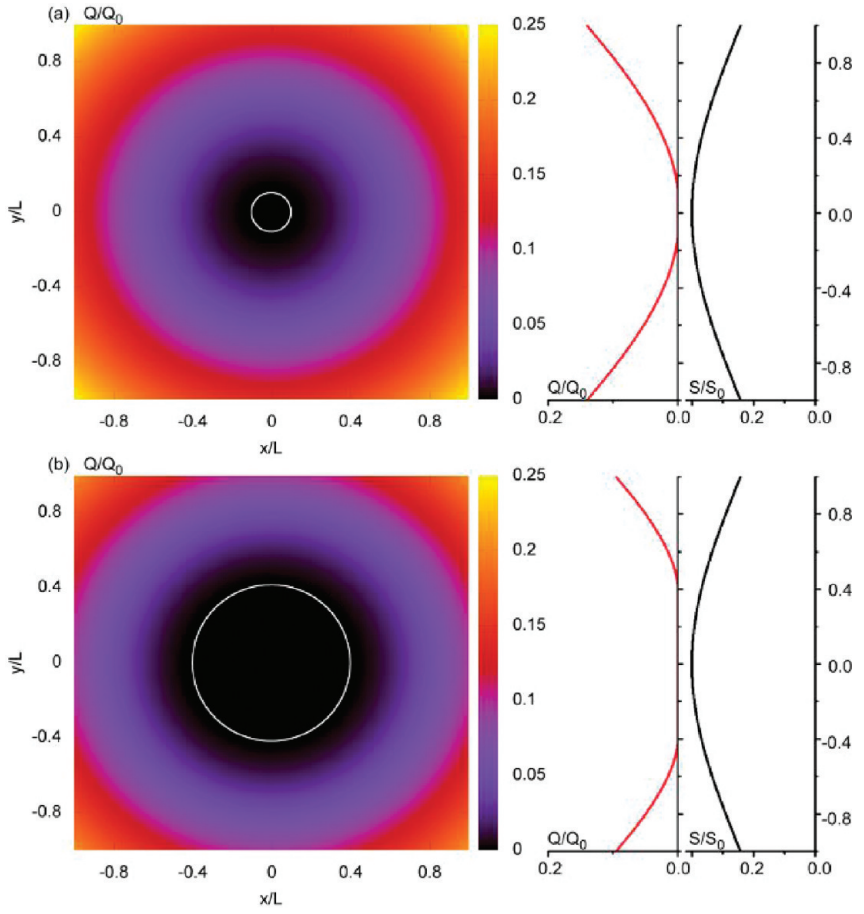

Figure 8. Calculated distributions of the quencher number density Q with respect to the initial quencher number density Q_0 (color maps and red line graphs). L is the width of the Gaussian radical source. Radii of the quencher-free domains (indicated with white circles) are 0.1L (a) and 0.4L (b). Ratio of the magnitudes of the laser beam intensity between cases (b) and (a) is $I_b/I_a \approx 1.038$. The distributions of the source of the radicals are plotted with black lines.

It can be seen that there is no quencher in the central domain of the irradiated volume. The polymerization is inhibited only in the region that surrounds this domain. This effect is similar to the one reached in STED-DLW; however, in our case, one does not need any depletion beam.

By solving eqs 1 and 2 for the case of Gaussian radical source 4 one can analytically obtain the radius of the quencher-free domain:

$$r_1 = L\sqrt{2\ln\left(\frac{S_0 L^2}{Q_0 D_Q}\right)} \qquad (5)$$

where Q_0 is initial quencher number density. It can be seen that the radius can be made arbitrarily small by tuning the laser beam intensity, since the radical source magnitude is $S \propto I^2(\vec{r},t)t_p R_p$. The irradiation time, conversely, does not affect the size of the quencher-free domain. An increase in the irradiation time (or a decrease in the scan speed) causes only an increase in the polymerization degree (conversion) within the quencher-free domain. In contrast, in the threshold model (without quencher diffusion), the maximal polymerization degree of a nanofeature can be increased by applying higher irradiation dose by increasing either beam intensity or irradiation time (Figure 9). However, the higher dose inevitably results in increase of the size of the polymer feature. By employing the diffusion of the quencher, one can handle both the size and the maximal conversion of the polymer feature separately. The formation of sharp spatial distributions of the conversion is important for

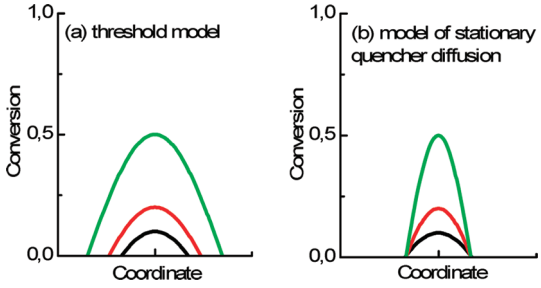

Figure 9. (a) Schematic representation of conversion profiles in threshold polymerization regime for different irradiation doses. (b) Schematic representation of conversion profiles in a model of stationary quencher diffusion for different irradiation times and fixed irradiation intensity.

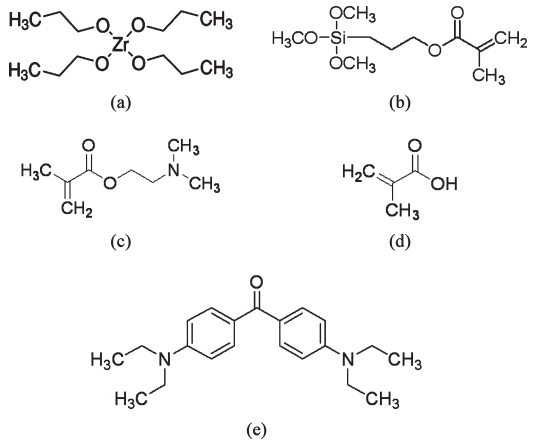

Figure 10. Chemicals used: (a) ZPO, (b) MAPTMS, (c) DMAEMA, (d) MAA, (e) BIS.

achieving high spatial resolution, high mechanical stability, and stability against fluctuations.[28]

The model presented above has not taken into account the temperature and gel viscosity, parameters that would increase and decrease the diffusivity of the quencher, respectively. In addition, the size of the quencher is a major factor; a smaller quencher would diffuse faster. A more detailed modeling of the polymerization with diffusing quencher is planned for a future publication.

This new method based on quencher diffusion does not possess the stringent material requirements of STED-DLW; it does, however impose certain limitations. The most important one is writing speed, as it is required that the laser scanning speed allows enough time for the quencher to diffuse. This could become an issue in the fabrication of larger structures if liquid photopolymers are used, due to thermal drift or other destabilizing factors. Fortunately, most hybrid materials, like the one used here, have gel form, and thermal drift or displacement is not a problem.

The low writing speed and therefore low efficiency problem could be addressed by using a faster diffusing quencher or by using a writing strategy of multiple scans. There, each layer of the structure could be scanned two or three times using fluence well below the polymerization threshold. During each scan, some monomer/oligomer units would polymerize, but not enough to provide a solid structure. During the time it takes to scan the whole layer, the quencher would diffuse. Eventually, after multiple scans, there would be enough polymerized material for the structure to survive development. We have carried out preliminary studies using multiple scans, and the results are similar to using a slow scanning speed. This, combined with other techniques such as multiple foci beams,[29] could substantially increase the productivity of this method.

CONCLUSIONS

We have presented our investigations into improving the resolution of three-dimensional structures by using a combination of a quenching monomer with slow laser scanning speed. We have fabricated woodpile structures with interlayer period 400 nm, comparable to what has been achieved by DLW-STED, considered today as "state-of-the-art". In addition, we have proposed a mechanism for this improved resolution. We have characterized the woodpile structures using angled-resolved transmission microscopy, and we have shown that they exhibit long-range periodicity and near-infrared stopgaps. The materials we use are readily available. While the method we propose does not allow the voxel shape control that DLW-STED does, we believe it offers an attractive alternative to high-resolution 3D photopolymer structuring.

EXPERIMENTAL SECTION

Materials. All the chemicals used in this work were obtained from Sigma-Aldrich and used without further purification.

The material used for the fabrication of the 3D structures is based on the organic−inorganic hybrid described earlier.[19,20] It has been produced by the addition of zirconium propoxide (Figure 10a, ZPO, 70% in propanol) to methacryloxypropyl trimethoxysilane (Figure 10b, MAPTMS). The monomer 2-(dimethylamino)ethyl methacrylate (Figure 10c, DMAEMA) has been added as a quencher. MAPTMS, methacrylic acid (Figure 10d, MAA), and DMAEMA were used as the organic photopolymerizable monomers, while ZPO and the alkoxysilane groups of MAPTMS served as the inorganic network forming moieties. Michler's ketone, 4,4-bis(diethylamino) benzophenone (Figure 10e, BIS), was used as a photoinitiator.

MAPTMS was first hydrolyzed using HCl solution (0.1 M) at a 1:0.1 ratio. ZPO was reacted with MAA (molar ratio 1:1). After 5 min, the zirconium complex was slowly added to the hydrolyzed MAPTMS at a 2:8 molar ratio. After stirring for 15 min, DMAEMA was added. The (MAPTMS+ZPO):DMAEMA molar ratio was 9:1. Finally, the photoinitiator, at a 1% w/w concentration, was added to the mixture. After stirring for a further 15 min, the composite was filtered using a 0.22 μm pore size syringe filter.

The samples were prepared by drop-casting onto 100 μm thick silanized glass substrates, and the resultant films were dried in an oven at 50 °C for 10 min before the photopolymerization. The heating process led to the condensation of the alkoxide groups and the formation of the inorganic matrix. Next, the organic moieties were polymerized using DLW, resulting in the formation of irreversible and fully saturated aliphatic C−C covalent bonds that further increased the connectivity of the material.

After the completion of the component build process by DLW, the samples were developed for 20 min in a 50:50 solution of 1-propanol/2-propanol and were further rinsed with 2-propanol.

3D Structure Fabrication. The experimental setup employed for 3D structure fabrication has been described previously.[30,31] A Ti:Sapphire femtosecond laser (Femtolasers Fusion, 800 nm, 75 MHz, <20 fs) was focused into the photopolymerizable composite using a high numerical aperture focusing microscope objective lens (100×, N.A. = 1.4, Zeiss, Plan Apochromat). Sample movement was achieved using piezoelectric and linear stages, for fine and step movement, respectively (Physik Instrumente). The whole DLW setup was computer-controlled using the 3DPoli software. The average power used for the fabrication of the high-resolution structures was 4.8 mW,

measured before the objective, while the average transmission was 20%. The scanning speed was always set to 20 μm/s.

Woodpile Structures. The photonic structures fabricated were photonic crystals using the woodpile geometry.[32,33] This consists of layers of one-dimensional rods with a stacking sequence that repeats itself every four layers. The distance between four adjacent layers is *c*, and, within each layer, the axes of the rods are parallel to each other with a distance *d* between them. The adjacent layers are rotated by 90°. Between every other layer, the rods are shifted relative to each other by *d*/2. For the case of $c/d = \sqrt{2}$, which was used in these experiments, the lattice can be derived from a face-centered-cubic unit cell with a basis of two rods.

Optical Characterization. *Refractive Index Measurements.* The refractive index of the thin films of the composite at 632.8 nm was determined from an m-line prism coupling experiment, using a He−Ne laser,[34,35] following the process described in ref 19. It was found to be 1.512 ± 0.006.

Angle-Resolved Transmittance Measurements. Since the contrast in refractive index between the material and air is on the order of 0.5, the fabricated woodpile crystals do not possess a complete photonic band gap. However, in certain directions a photonic stopgap arises leading to a decrease in transmission. The transmission spectra of the woodpile structure stopgaps were measured using angle-resolved transmittance microscopy. For this, a home-built setup was employed, built according to refs 36 and 37. Light from a Ti-Sapphire laser (800 nm, 180 fs, 1 mJ/pulse, 1 kHz repetition rate) was focused using an *f* = 3 cm lens into a 3 cm long cell filled with distilled water, in order to produce a white-light continuum, providing a useful broad spectral range of 450 to 1000 nm wavelength. The light was collimated and then focused on the sample. The sample was mounted to obtain accurate 3D and rotational control. Another lens was coupled with the beam and, in combination with a lens, imaged the sample onto an intermediate image plane. This intermediate image plane was further imaged onto a IR/vis fiber with a core diameter of 200 μm. The output of the fiber was connected to an optical spectrometer (Ocean Optics S2000), covering a spectral range from 300 to 1000 nm. The spectrum was recorded through a Labview-driven program. To ensure proper normalization, all the measured transmission spectra were normalized to the bare glass substrate for the same angle of incidence, requiring only a very small lateral movement of the sample. In order to align the sample appropriately on the optical axis, the intermediate image plane was imaged onto a CCD camera using a dichroic mirror. This also served to remove the 800 nm pump laser beam of the continuum, thus avoiding saturation of the spectrum analyzer. The half-opening angle of the incident light was reduced to 5°, assured by iris diaphragms.

The diameter of the beam at the sample was 6 μm, while the measured nanostructure surface normal to the beam was typically 30 μm × 30 μm. As the size of the sample's surface is comparable to the beam spot diameter, sample alignment is difficult and critical. To check the alignment, but also to check the quality of the sample, the diffraction patterns in the transmitted waves produced by the structure when illuminated by the white light beam were used. In general, diffraction patterns reveal structural characteristics, as well as sample quality. Figure 2c shows a typical diffraction pattern, generated by the woodpile structure of Figure 2a,b (SEM image, full structure and detail). To understand the diffraction pattern, one should note that the woodpile structure presents the {001} family of planes parallel to the crystal surface; the direction normal to these planes is referred as ΓX, which is the one studied. In these planes the structure presents a square symmetry, which is actually revealed by the square symmetry of the diffraction pattern observed.[24]

Conflict of Interest: The authors declare no competing financial interest.

Acknowledgment. This work was partly funded by the ITN TOPBIO (PITN-GA-2010-264362). V.P. was supported by the EU Marie Curie Fellowship Program: FASTQUAST (PITN-GA-2008-214962). A.P. and N.B. were supported in part by Federal Targeted Program "Scientific and Scientific-Pedagogical Personnel of the Innovative Russia" under Contract Nos. 16.740.11.0656 and 16.740.11.0018, by RFBR under Grant Nos. 09-02-00665-a and 11-02-97053-r_povoljie_a, and by the Program of Presidium of the Russian Academy of Sciences "Extreme Light Fields and Applications". We would like to thank Mrs. Aleka Manousaki for expert technical assistance with SEM.

REFERENCES AND NOTES

1. Juodkazis, S.; Mizeikis, V.; Misawa, H. Three-Dimensional Microfabrication of Materials by Femtosecond Lasers for Photonics Applications. *J. Appl. Phys.* **2009**, *106*, 051101.
2. Soukoulis, C. M.; Wegener, M. Past Achievements and Future Challenges in the Development of Three-Dimensional Photonic Metamaterials. *Nat. Photonics* **2011**, *5*, 523–530.
3. Schizas, C.; Melissinaki, V.; Gaidukeviciute, A.; Reinhardt, C.; Ohrt, C.; Dedoussis, V.; Chichkov, B. N.; Fotakis, C.; Farsari, M.; Karalekas, D. On the Design and Fabrication by Two-Photon Polymerization of a Readily Assembled Micro-Valve. *Int. J. Adv. Manufact. Technol.* **2010**, *48*, 435–441.
4. Farsari, M.; Vamvakaki, M.; Chichkov, B. N. Multiphoton Polymerization of Hybrid Materials. *J. Opt.* **2010**, *12*, 124001.
5. Grossmann, T.; Schleede, S.; Hauser, M.; Beck, T.; Thiel, M.; von Freymann, G.; Mappes, T.; Kalt, H. Direct Laser Writing for Active and Passive High-Q Polymer Microdisks on Silicon. *Opt. Exp.* **2011**, *19*, 11451–11456.
6. Malinauskas, M.; Zukauskas, A.; Bickauskaite, G.; Gadonas, R.; Juodkazis, S. Mechanisms of Three-Dimensional Structuring of Photo-Polymers by Tightly Focussed Femtosecond Laser Pulses. *Opt. Exp.* **2010**, *18*, 10209–10221.
7. Lu, W.-E.; Dong, X.-Z.; Chen, W.-Q.; Zhao, Z.-S.; Duan, X.-M. Novel Photoinitiator with a Radical Quenching Moiety for Confining Radical Diffusion in Two-Photon Induced Photopolymerization. *J. Mater. Chem.* **2011**, *21*, 5650–5659.
8. Abbe, E. Theorie des Mikroskops und der Mikroskopischen Wahrnehmung. *Arch. Microskop. Anat.* **1873**, 413–468.
9. Born, M.; Wolf, E. *Principles of Optics*, 7th ed.; Cambridge University Press: Cambridge, 1999.
10. Park, S. H.; Lim, T. W.; Yang, D. Y.; Kim, R. H.; Lee, K. S. Improvement of Spatial Resolution in Nano-Stereolithography Using Radical Quencher. *Macromol. Res.* **2006**, *14*, 559–564.
11. Fischer, J.; Wegener, M. Three-Dimensional Direct Laser Writing Inspired by Stimulated-Emission-Depletion Microscopy. *Opt. Mater. Express* **2011**, *1*, 614–624.
12. Pikulin, A.; Bityurin, N. Spatial Resolution in Polymerization of Sample Features at Nanoscale. *Phys. Rev. B* **2007**, *75*, 195430.
13. Hell, S. W.; Wichmann, J. Breaking the Diffraction Resolution Limit by Stimulated Emission: Stimulated-Emission-Depletion Fluorescence Microscopy. *Opt. Lett.* **1994**, *19*, 780–782.
14. Klar, T. A.; Jakobs, S.; Dyba, M.; Egner, A.; Hell, S. W. Fluorescence Microscopy with Diffraction Resolution Barrier Broken by Stimulated Emission. *Proc. Natl. Acad. Sci. U. S. A.* **2000**, *97*, 8206–8210.
15. Scott, T. F.; Kowalski, B. A.; Sullivan, A. C.; Bowman, C. N.; McLeod, R. R. Two-Color Single-Photon Photoinitiation and Photoinhibition for Subdiffraction Photolithography. *Science* **2009**, *324*, 913–917.
16. Li, L. J.; Gattass, R. R.; Gershgoren, E.; Hwang, H.; Fourkas, J. T. Achieving lambda/20 Resolution by One-Color Initiation and Deactivation of Polymerization. *Science* **2009**, *324*, 910–913.
17. Cao, Y.; Gan, Z.; Jia, B.; Evans, R. A.; Gu, M. High-Photosensitive Resin for Super-Resolution Direct-Laser-Writing Based on Photoinhibited Polymerization. *Opt. Express* **2011**, *19*, 19486–19494.
18. Wolf, T. J. A.; Fischer, J.; Wegener, M.; Unterreiner, A. N. Pump-Probe Spectroscopy on Photoinitiators for Stimulated-Emission-Depletion Optical Lithography. *Opt. Lett.* **2011**, *36*, 3188–3190.

19. Ovsianikov, A.; Viertl, J.; Chichkov, B.; Oubaha, M.; MacCraith, B.; Sakellari, L.; Giakoumaki, A.; Gray, D.; Vamvakaki, M.; Farsari, M.; Fotakis, C. Ultra-Low Shrinkage Hybrid Photosensitive Material for Two-Photon Polymerization Microfabrication. *ACS Nano* **2008**, *2*, 2257–2262.
20. Ovsianikov, A.; Xiao, S. Z.; Farsari, M.; Vamvakaki, M.; Fotakis, C.; Chichkov, B. N. Shrinkage of Microstructures Produced by Two-Photon Polymerization of Zr-based Hybrid Photosensitive Materials. *Opt. Express* **2009**, *17*, 2143–2148.
21. Sun, Q.; Juodkazis, S.; Murazawa, N.; Mizeikis, V.; Misawa, H. Freestanding and Movable Photonic Microstructures Fabricated by Photopolymerization with Femtosecond Laser Pulses. *J. Micromech. Microeng.* **2010**, 035004.
22. Terzaki, K.; Vasilantonakis, N.; Gaidukeviciute, A.; Reinhardt, C.; Fotakis, C.; Vamvakaki, M.; Farsari, M. 3D Conducting Nanostructures Fabricated Using Direct Laser Writing. *Opt. Mater. Express* **2011**, *1*, 586–597.
23. Vasilantonakis, N.; Terzaki, K.; Sakellari, I.; Purlys, V.; Gray, D.; Soukoulis, C. M.; Vamvakaki, M.; Kafesaki, M.; Farsari, M. Three-Dimensional Metallic Photonic Crystals with Optical Bandgaps. *Adv. Mater.* **2012**, 10.1002/adma.201104778.
24. Roundy, D.; Joannopoulos., J. Photonic Crystal Structure with Square Symmetry within Each Layer and a Three-Dimensional Band Gap. *Appl. Phys. Lett.* **2003**, *82*, 3835–3837.
25. García-Santamaría, F.; Galisteo-López, J. F.; Braun, P. V.; López., C. Optical Diffraction and High-Energy Features in Three-Dimensional Photonic Crystals. *Phys. Rev. B* **2005**, *71*, 195112.
26. Dorado, L. A.; Depine, R. A.; Schinca, D.; Lozano, G.; Míguez, H. Experimental and Theoretical Analysis of the Intensity of Beams Diffracted by Three-Dimensional Photonic Crystals. *Phys. Rev. B* **2008**, *78*, 075102.
27. Johnson, S. G.; Joannopoulos, J. D. Block-Iterative Frequency-Domain Methods for Maxwell's Equations in a Planewave Basis. *Opt. Express* **2001**, *8*, 173–190.
28. Pikulin, A.; Bityurin, N. Spatial Confinement of Percolation: Monte Carlo Modeling and Nanoscale Laser Polymerization. *Phys. Rev. B* **2010**, *82*, 085406.
29. Obata, K.; Koch, J.; Hinze, U.; Chichkov, B. N. Multi-focus Two-Photon Polymerization Technique Based on Individually Controlled Phase Modulation. *Opt. Express* **2010**, *18*, 17193–17200.
30. Claeyssens, F.; Hasan, E. A.; Gaidukeviciute, A.; Achilleos, D. S.; Ranella, A.; Reinhardt, C.; Ovsianikov, A.; Xiao, S.; Fotakis, C.; Vamvakaki, M.; *et al*. Three-Dimensional Biodegradable Structures Fabricated by Two-Photon Polymerization. *Langmuir* **2009**, *25*, 3219–3223.
31. Sakellari, I.; Gaidukeviciute, A.; Giakoumaki, A.; Gray, D.; Fotakis, C.; Farsari, M.; Vamvakaki, M.; Reinhardt, C.; Ovsianikov, A.; Chichkov, B. N. Two-Photon Polymerization of Titanium-Containing Sol-Gel Composites for Three-Dimensional Structure Fabrication. *Appl. Phys. A: Mater. Sci. Process.* **2010**, *100*, 359–364.
32. Ho, K. M.; Chan, C. T.; Soukoulis, C. M.; Biswas, R.; Sigalas, M. Photonic Band Gaps in Three Dimensions: New Layer-by-Layer Periodic Structures. *Solid State Commun.* **1994**, *89*, 413–416.
33. Sigalas, M. M.; Ho., K. M.; Soukoulis, C. M.; Biswas, R.; Tuttle, G. Photonic Crystals. In *Wiley Encyclopedia of Electrical and Electronics Engineering*; Webster, J. G., Ed.; J. Wiley: New York, 1999.
34. Tien, P. K.; Smolinsky, G.; Martin, R. J. Thin Organosilicon Films for Integrated Optics. *Appl. Opt.* **1972**, *11*, 637–642.
35. Monneret, S.; Huguet-Chantôme, P.; Flory, F. m-lines Technique: Prism Coupling Measurement and Discussion of Accuracy for Homogeneous Waveguides. *J. Opt. A: Pure Appl. Opt.* **2000**, *2*, 188–195.
36. Deubel, M. Doctoral thesis: Three-Dimensional Photonic Crystals via Direct Laser Writing: Fabrication and Characterization. Universitat Karlsruhe, 2006.
37. Deubel, M.; Wegener, M.; Linden, S.; von Freymann, G. Angle-Resolved Transmission Spectroscopy of Three-Dimensional Photonic Crystals Fabricated by Direct Laser Writing. *Appl. Phys. Lett.* **2005**, *87*, 221104.